Excitonic Coupling of Chlorophylls in the Plant Light-Harvesting Complex LHC-II

Axel Schubert,* Wichard J. D. Beenken,† Holger Stiel,† Bernd Voigt,† Dieter Leupold,† and Heiko Lokstein*
*Humboldt-Universität zu Berlin, Institut für Biologie Plant Physiology, Unter den Linden 6, D-10099 Berlin, and †Max-Born-Institut für Nichtlineare Optik und Kurzzeitspektroskopie, D-12489 Berlin, Germany

ABSTRACT Manifestation and extent of excitonic interactions in the red Chl-absorption region (Q_y band) of trimeric LHC-II were investigated using two complementary nonlinear laser-spectroscopic techniques. Nonlinear absorption of 120-fs pulses indicates an increased absorption cross section in the red wing of the Q_y band as compared to monomeric Chl *a* in organic solution. Additionally, the dependence of a nonlinear polarization response on the pump-field intensity was investigated. This approach reveals that one emitting spectral form, characterized by a 2.3(±0.8)-fold larger dipole strength than monomeric Chl *a*, dominates the fluorescence spectrum of LHC-II. Considering available structural and spectroscopic data, these results can be consistently explained assuming the existence of an excitonically coupled dimer located at Chl-bindings sites **a2** and **b2** (referring to the original notation of W. Kühlbrandt, D. N. Wang, and Y. Fujiyoshi, *Nature*, 1994, 367:614–621), which must not necessarily correspond to Chls *a* and *b*). This fluorescent dimer, terminating the excitation energy-transfer chain of the LHC-II monomeric subunit, is discussed with respect to its relevance for intra- and inter-antenna excitation energy transfer.

INTRODUCTION

Higher plants possess an intricate light-harvesting antenna system for effective capture of photons and excitation energy transfer (EET) to the reaction centers of both photosystems I and II. The bulk antenna is the mainly photosystem II-associated light-harvesting complex (LHC-II) harboring ~50% of the total chlorophyll (Chl) *a* + *b* in plant thylakoid membranes. A structural model for trimeric LHC-II, as obtained by electron crystallography at 3.4-Å resolution, reveals that 12 Chls (7 Chls *a* + 5 Chls *b*) are attached to each monomeric subunit (Kühlbrandt et al., 1994). The shortest center-to-center distances between Chls in the model range from 8 to 14 Å, thus rendering the existence of excitonic interactions among pigments highly likely. However, at the current structural resolution, Chls *a* and *b* are not directly distinguishable, although the occupation of some Chl-binding sites has been recently verified by site-directed mutagenesis (Remelli et al., 1999; Rogl and Kühlbrandt, 1999). Moreover, orientations of the Chl transition-dipole moments within the molecular planes cannot be determined unambiguously, and, hence, they are a matter of continuing debate (van Amerongen and van Grondelle, 2001). Therefore, estimation of excitonic coupling from available structure data is still unreliable.

Regarding effective EET as one main task of an antenna system, dipole–dipole interactions between Chls functions as the key mechanism. Strong electronic coupling among pigments, forming a more or less delocalized exciton, may increase the EET efficiency (van Grondelle, 1985). In this case, the exciton energy levels are commonly shifted in comparison to the excited state energies of monomeric Chls. However, interactions of the Chls with their protein environment can cause similar spectral shifts (Nishigaki et al., 2001). The consistent understanding of the LHC-II absorption in an overall substructure model, including possible excitonic effects, is thus complicated by the unknown origin of the observed spectral heterogeneity of at least 10 subbands (Nussberger et al., 1994). Another significant feature of excitonic coupling is that light-induced bleaching of one exciton state affects the spectral distributions of the other one. Accordingly, the occurrence of satellite holes in nonphotochemical hole-burning experiments at 4 K has been taken as indicative of excitonic coupling (Reddy et al., 1994). Unfortunately, this effect cannot be distinguished sufficiently from burning-induced alterations in the protein matrix, and the hole-burning technique additionally suffers from requiring low temperatures. Excitonic interaction is further reflected by considerably increased optical activity (van Amerongen et al., 2000). Compared to monomeric Chl in solution, circular dichroism spectra of LHC-II reveal a rotational strength that may hardly be explained without considering excitonic interactions (Hemelrijk et al., 1992). Nevertheless, considerable nonconservative contributions to the circular dichroism spectrum of LHC-II and the large number of involved subbands have hindered consistent modeling of these spectra so far.

Here, we present a new approach to assess excitonic coupling between Chls by probing the redistribution of optical transition probability directly. Recently, Leupold et al. (1996, 1999) have applied nonlinear absorption spectroscopy (NLA) to elucidate the extent of excitonic coupling in the peripheral antenna complex (LH2) of the purple bacterium *Rhodobacter sphaeroides*. The technique (using picosecond pulses) facilitated the detection of considerably size-

Submitted July 18, 2001 and accepted for publication October 24, 2001.

Drs. Schubert's and Beenken's present address is Dept. of Chemical Physics, Lund University, P.O. Box 124, SE-22100 Lund, Sweden.

Address reprint requests to Axel Schubert, Dept. of Chemical Physics, Lund University, P.O. Box 124, SE-22100 Lund, Sweden. Tel.: +46-46-2224739; Fax: +46-46-2224119; E-mail: axel.schubert@chemphys.lu.se.

0006-3495/02/02/1030/10 $2.00

enhanced transition-dipole moments. However, the much more complicated spectral substructure and excitation dynamics in LHC-II do not allow the straightforward evaluation of similar NLA experiments. Hence, the NLA technique was used with 120-fs laser pulses to investigate manifestation and extent of excitonic interactions in the Q_y-absorption band of trimeric LHC-II. Applicability of this approach to the problem was established in previously performed NLA experiments with monomeric Chl *a* and Chl *a* aggregates in organic solution comparing data obtained using 120-fs and 400-ps pulses (Schubert et al., 1998).

Nonlinear polarization spectroscopy in the frequency domain (NLPF) was used to gain additional insight. Previous NLPF studies of LHC-II (Lokstein et al., 1995; Schubert et al., 1997) were evaluated in the framework of a weak-field approximation (Song et al., 1978; Beenken and Ehlert, 1998). In the current study, the intensity dependence of NLPF spectra is used to determine the emission cross section in a certain spectral region. This approach is based on the strong-field theory of NLPF as introduced by Beenken and May (1997). Notably, both techniques rely on complementary attempts to simplify the theoretical handling of the underlying systems dynamics. Although NLA, with femtosecond pulses, represents a quasi-instantaneous approach, the model used here to interpret NLPF data is based on the assumption of quasi-stationary conditions after completion of the fast EET processes.

MATERIALS AND METHODS

LHC-II was isolated from freshly harvested pea leaves following the procedure of Krupa et al. (1987). LHC-II in the trimeric state was obtained in a buffer containing 10 mM Tricine (pH 7.8) and 1.2% *n*-octyl β-D-glucopyranoside at 110 μg/ml Chl *a* + *b*. Absorption and fluorescence spectra were measured before and after the laser-spectroscopic experiments to monitor integrity of the samples.

The NLA experiment registers sample transmission in dependence on incident light intensity in a single beam set-up as described previously (Stiel et al., 1991a). The femtosecond laser system (CPA 1000, CLARK-MXR Inc., Dexter, MI) provides 120-fs pulses with a spectral width of 6 nm full-width-at-half-maximum (FWHM) as monitored by a frequency-resolved optical gating analyzer (Clark-MXR Inc.). The laser beam was focused onto a 1-mm rotating sample cuvette (Hellma, Mülheim, Germany) to a spot of 30-μm diameter. Intensity was varied using a neutral-density filter wheel. NLA data analysis was performed with the software package CALE (Stiel et al., 1991b).

Intensity-dependent NLPF spectra were recorded applying a 90° arrangement of pump and probe laser beams (Fig. 1) as introduced recently (Voigt et al., 1999). Both laser beams (spectral widths of ~5 pm) are obtained from dye lasers (DCM in DMSO) simultaneously pumped by excimer laser pulses (15 ns).

RESULTS

Nonlinear absorption

First, we present the results of the NLA experiment with trimeric LHC-II. Application of the NLA technique using

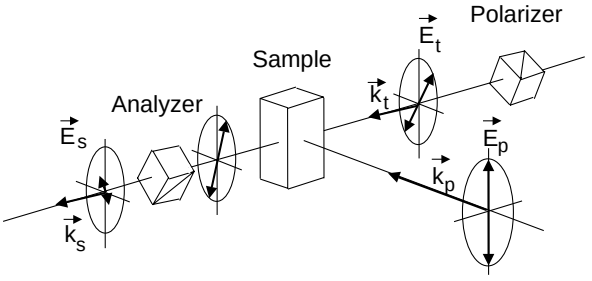

FIGURE 1 Set-up (schematic) for NLPF. Pump, probe, and signal fields ($\vec{E}$) and the corresponding wave number vectors ($\vec{k}$) are distinguished by the indices p, t, and s. The NLPF signal is the component of the signal field perpendicular to the incident probe field. A more extensive description of the NLPF technique can be found in Voigt et al. (1999).

120-fs pulses at the red edge of the Q_y-absorption band benefits from a pulse duration that is short as compared to the fastest energy-relaxation processes observed in the covered spectral region (compare, e.g., EET rates reported in Trinkunas et al., 1997). This allows us to neglect incoherent EET dynamics, resulting in essential simplifications of the theoretical model for interpretation of the NLA data. Moreover, a possibly unresolved relaxation among exciton states (coherent EET) can also be excluded, because, in the case of efficient excitonic coupling, the upper exciton bands are not sufficiently populated due to their spectral separation. In contrast, the spectral width of the 120-fs pulse (6 nm, FWHM) increases the error range in a spectrally integrating NLA experiment and, hence, favors its application in regions of moderate absorption changes. The most reasonable compromise between these two requirements was established by applying femtosecond pulses at a central wavelength of 680 nm (see Fig. 2).

Being able to neglect the EET dynamics, the obtained NLA curve (Fig. 3) can be evaluated on the basis of a three-level model. The model includes absorption from the ground state (S_0) to the first excited singlet state (S_1) and from there to a higher excited singlet state, S_x. It should be mentioned that this model does not distinguish between exciton states of excitonically coupled molecules or transitions of monomeric molecules. The remaining time constants in this system are the lifetimes of S_1 and S_x. Whereas the S_1 lifetime in LHC-II (3.6 ns) is infinitely long with respect to the laser pulse duration, the latter might be much faster due to rapid internal conversion. To the best of our knowledge, no precise S_x internal conversion rates are available for Chls *a* and *b*. However, related molecules (e.g., Zn-porphyrin) show time constants well above one picosecond (Cho et al., 2000). Because S_x-lifetimes longer than one picosecond are insignificant for fitting NLA data obtained with 120-fs pulses, the entire model can be reduced to a quasi-instantaneous approach (i.e., without having to consider rate constants).

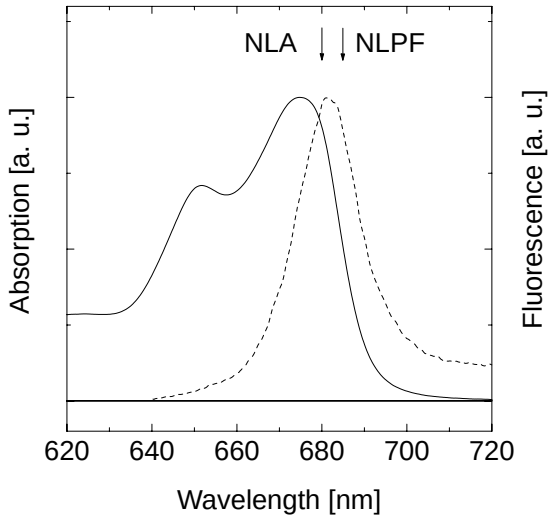

FIGURE 2 Q_y absorption (*solid line*) and fluorescence (excitation at 650 nm, *dashed line*) spectra of trimeric LHC-II. Arrows indicate spectral positions of the NLA measurement and the probe wavelength used for intensity-dependent NLPF.

Under these assumptions, the NLA curve representing the intensity-dependent transmission $T(I)$ can be expressed as

$$T(I) = \int I(t)\exp[c(\sigma_{10}^{abs}(n_1(t) - n_0(t)) + \sigma_{x1}^{abs}(n_x(t) - n_1(t)))d]\,dt \Big/ \int I(t)\,dt, \quad (1)$$

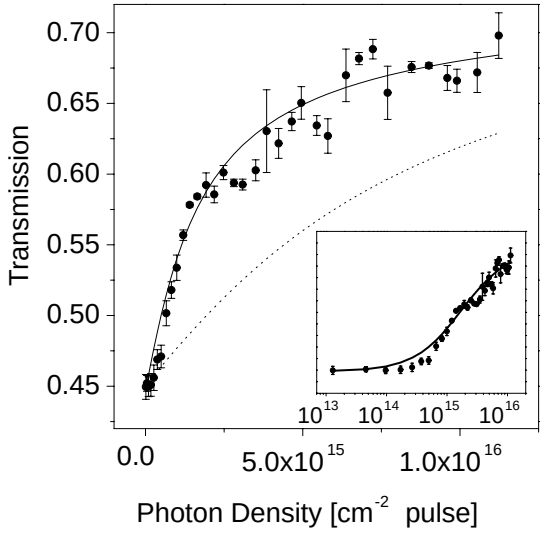

FIGURE 3 Nonlinear absorption (intensity-dependent transmission) of trimeric LHC-II at 680 nm. The solid line represents the best fit to the experimental data (for parameters, see text). The insert shows the same curves in logarithmic intensity representation. The dashed line is a simulation for comparison to monomeric Chl *a* using the value of 3.1×10^{-16} cm^2 for both ground and excited-state absorption cross section.

where the populations $n_i(t)$ are described by the system of differential equations,

$$\frac{dn_i(t)}{dt} = \sum_j \sigma_{ij}^{abs}(n_j(t) - n_i(t))I(t), \quad (2)$$

with the initial conditions $n_i(t_0) = \delta_{i0}$. $I(t)$ is the incident time-dependent light intensity, which is approximated as Gaussian shaped. The quantities c and d represent the particle density of LHC-II and the optical path length in the sample, respectively. σ_{ij} is the absorption cross section of the transition from state j to i and is assumed here to be equal to the corresponding cross section for stimulated emission from i to j. The spatial dependency of $I(t)$ by absorption is accounted for by the photon transport equation (see Stiel et al., 1991b). In the quasi-instantaneous approach, the NLA curve depends only on σ_{ij}. Fitting the NLA curve displayed in Fig. 3 yields a ground-state absorption cross section of $1.3(\pm 0.2) \times 10^{-15}$ cm^2 at 680 nm for LHC-II (and $1.5(\pm 0.2) \times 10^{-15}$ cm^2 for excited state absorption). This value is about four times that of monomeric Chl *a* in diethyl-ether solution (3.1×10^{-16} cm^2 at peak wavelength, compare Shipman, 1977).

For evaluation of NLA data obtained at wavelengths shorter than 680 nm, one would have to consider EET on time scales of the laser-pulse duration, even using 120-fs pulses (Trinkunas et al., 1997). Several attempts of summarizing measured EET rates in an overall scheme were made recently (Gradinaru et al., 1998; Agarwal et al., 2000), but no generally accepted model has been established so far. Therefore, analysis of NLA data obtained at shorter wavelengths is less straightforward and was omitted here.

Intensity-dependent nonlinear polarization spectroscopy

NLPF spectra of LHC-II obtained at different probe wavelengths with low pump-beam intensities have been presented and discussed previously (Lokstein et al., 1995, 1998). Here, we focus on intensity-dependent NLPF spectra recorded with the probe wavelength fixed in the spectral region of LHC-II fluorescence (685 nm, see Fig. 2). The pump wavelength was tuned across the (overlapping) Chl *a* absorption and emission regions (670–690 nm). NLPF spectra recorded at different pump-beam intensities are presented in Fig. 4. Each curve is the average of 10 repetitive measurements, additionally smoothed by averaging over 15 neighboring data points. The distribution of data points before smoothing is shown for curve *d*. For the pump-beam intensities used, see the legend of Fig. 4. At every pump wavelength λ_p, the intensity dependence of the NLPF signal was extracted from curves *a*–*g*. This is illustrated in Fig. 5 for $\lambda_p = 678$ nm (corresponding to the dashed line in Fig. 4).

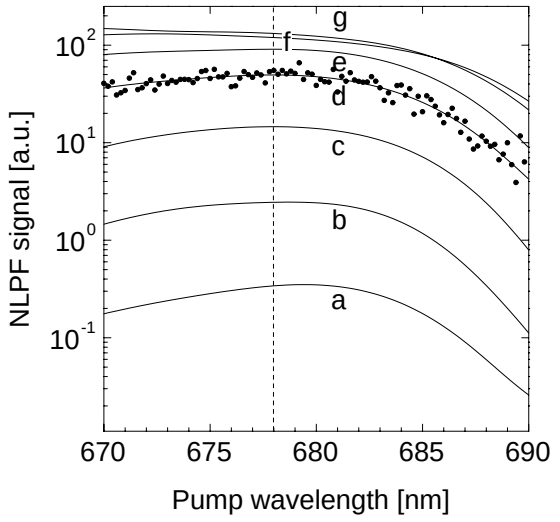

FIGURE 4 NLPF spectra of trimeric LHC-II probed at 685 nm for different pump-field intensities: (*a*) 5.7×10^{21}, (*b*) 2.3×10^{22}, (*c*) 8.0×10^{22}, (*d*) 2.1×10^{23}, (*e*) 4.7×10^{23}, (*f*) 1.4×10^{24}, and (*g*) 4.3×10^{24} photons $cm^{-2}\ s^{-1}$. Solid lines represent smoothed spectra (see text), dots indicate original distribution of the data belonging to curve *d*. NLPF signal values as obtained at a pump wavelength of 678 nm (*vertical line*) are used to demonstrate the intensity dependence in Fig. 5.

In agreement with the knowledge about EET processes in LHC-II (Connelly et al., 1997; Trinkunas et al., 1997; Gradinaru et al., 1998), the model for evaluation of the spectra can be based on the assumption that all excitations are transferred to the fluorescent state(s) on a time scale significantly shorter than the fluorescence lifetime. Thus, unknown intermediate steps in the EET scheme can be neglected, and the system can be described in a generalized donor/acceptor model. As deduced in the appendix, the intensity dependence of the NLPF signal for probing the fluorescent state (acceptor) is determined by Eq. A8, depending on only two parameters $\xi(\omega_p)$ and $\eta(\omega_p, \omega_t)$. Here the reciprocal value of the saturation parameter $\xi(\omega_p)$ indicates the point at which the NLPF signal starts to deviate from the initial quadratic intensity dependence. The large number of Chls in LHC-II requires the consideration of several donors and acceptors and, additionally, branched EET between them. Therefore the model was extended, resulting in Eq. A9 for the saturation parameter, which can also be expressed as

$$\xi(\omega_p) = \frac{\sigma^{abs}(\omega_p)}{N_A \cdot \gamma_{fd}} + \frac{\sigma^{em}(\omega_p)}{N_A \cdot \gamma_{fd}}. \qquad (3)$$

Here, the cross section $\sigma^{abs}(\omega_p)$ does not necessarily reproduce the steady-state absorption spectrum of LHC-II. Rather, $\sigma^{abs}(\omega_p)$ comprises the absorption of the probed acceptor(s) and of those donors that confer their excitation energy to them (compare Eq. A9). Analogously, the cross section $\sigma^{em}(\omega_p)$ may not reflect the entire fluorescence spectrum but only the emission of the probed acceptor state(s). The fluorescence decay rate γ_{fd} has to be multiplied by the number of fluorescent species N_A if the EET path branches to more than one acceptor. The second parameter $\eta(\omega_p)$ is determined by the ratio between γ_{fd} and the EET rates according to Eq. A7. Thus, $\eta(\omega_p)$ is ideally suited to verify the assumption of EET being much faster than the fluorescence decay.

NLPF saturation curves are fitted according to Eq. A8 to obtain values of $\xi(\omega_p)$ and $\eta(\omega_p)$. For the curve in Fig. 5, the fit yields the following parameters: $\xi = 8.4 \times 10^{-24}\ cm^2\ s$, $Re\{\eta\xi\} = 2.7 \times 10^{-26}\ cm^2\ s$ and $Im\{\eta\xi\} \approx 0$. The very low value of η implies that the EET rates γ_{AD} are significantly higher than the fluorescence decay rate γ_A according to Eq. A7. Plotting ξ versus λ_p, a "ξ-spectrum" was generated (Fig. 6).

A recent study on the bleaching behavior and fluorescence polarization of single complexes demonstrated that each of the three subunits in trimeric LHC-II is characterized by its own terminal acceptor state(s), thus suggesting a mainly independent EET path for each monomer (Tietz et al., 2001). Hence, the subunits of the trimer are expected to act independently in the NLPF experiment, too, and modeling has to account for the contributions of 7 Chl *a* and 5 Chl *b* comprising a monomeric subunit of LHC-II (Kühlbrand et al., 1994).

First, we estimate the contribution of $\sigma^{abs}(\omega_p)$ to the ξ-spectrum. Assuming that all donor species absorbing between 670 and 690 nm transfer their excitation energy to the probed acceptor(s), $\sigma^{abs}(\omega_p)$, as used in Eq. 3, equals the actual absorption cross section in this range. The total transition dipole strength of one LHC-II monomer yields

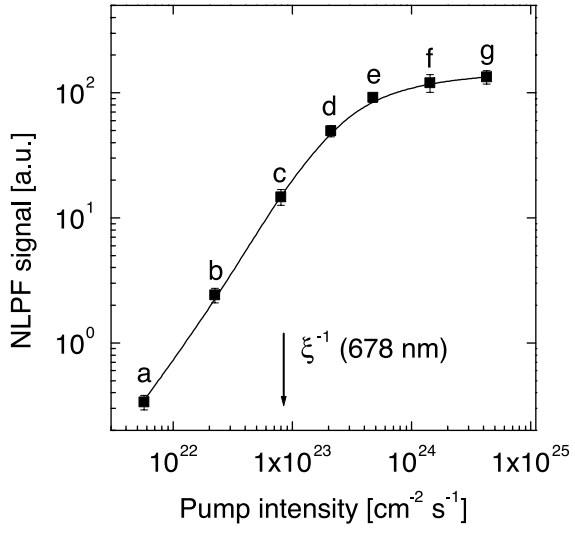

FIGURE 5 Intensity dependence of the NLPF signal of trimeric LHC-II probed at 685 nm and pumped at 678 nm as obtained from Fig. 4. The pump-beam intensities correspond to the values *a*–*g* given in the legend of Fig. 4. The solid line is the result of the fit (for parameters see text). The obtained ξ-value is visualized by an arrow.

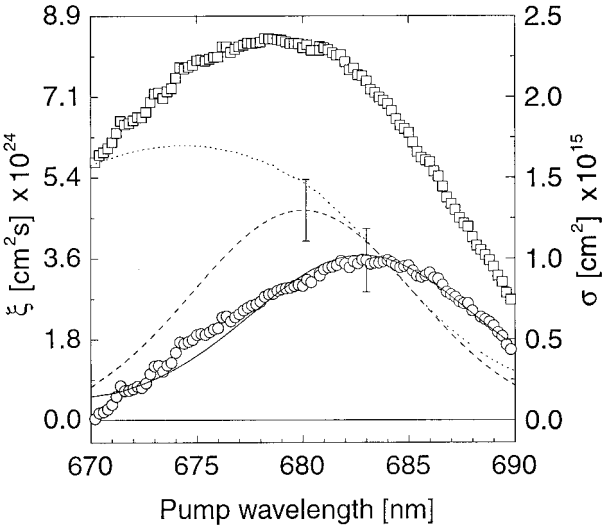

FIGURE 6 ξ-spectrum of trimeric LHC-II constructed from the intensity-dependent NLPF spectra in Fig. 4 (*squares*, *left scale*). The right scale (σ) is calculated from ξ by multiplication with the fluorescence decay rate $(3.6\ \text{ns})^{-1}$ (corresponding to the case $N_A = 1$ in Eq. 3, see text). Subtracting σ^{abs} (*dotted line*) from the ξ-spectrum yields σ^{em} (*circles*) of the terminal acceptor. Bars indicate the total statistical error. σ^{em} can be fitted by a Gaussian (*solid line*) centered at 683($\pm$1) nm with a FWHM of 260($\pm$30) cm^{-1}. For comparison with the NLA results, an absorption band with the same FWHM (260 cm^{-1}) and a maximum absorption cross section of 1.3×10^{-15} centered at 680 nm was simulated (*dashed line*).

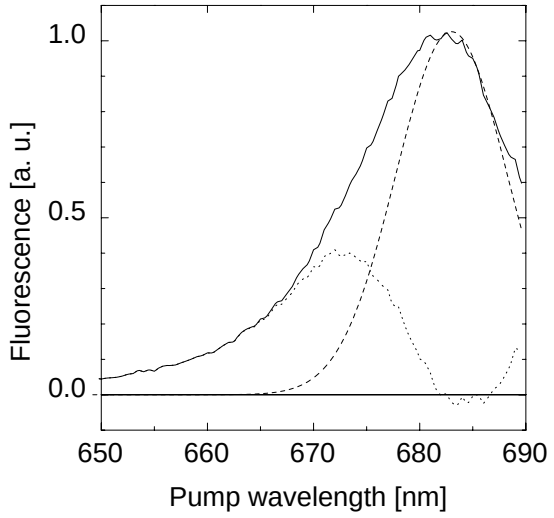

FIGURE 7 Deconvolution of the fluorescence spectrum (*solid line*) between 670 and 690 nm into a Gaussian subband (*dashed line*) at 683 nm with a FWHM of 260 cm^{-1} (cf. Fig. 6) and additional fluorescence band(s) with a maximum ~672 nm (*dotted line*).

$|\vec{\mu}_{LHC}|^2 = 7|\vec{\mu}_{Chla}|^2 + 5\,|\vec{\mu}_{Chlb}|^2 \approx 10.5|\vec{\mu}_{Chla}|^2$ considering $\vec{\mu}_{Chlb} \approx 0.83\ \vec{\mu}_{Chla}$ (Sauer et al., 1966). Scaling the area under the Q_y-absorption spectrum of LHC-II to the 10.5-fold of the area under the absorption cross section spectrum of Chl *a* (3.1×10^{-16} cm^2 at maximum, Shipman, 1977) yields σ^{abs} (674 nm) = $1.7(\pm0.3) \times 10^{-15}$ cm^2. This result can be used to gauge the LHC-II absorption spectrum between 670 and 690 nm to approximate values of $\sigma^{abs}(\omega_p)$.

Using this approach, the number of acceptors can be determined. In Fig. 6, the ξ-spectrum multiplied by $\gamma_{fd} = (3.6\ \text{ns})^{-1}$ is compared to $\sigma^{abs}(\omega_p)$ as approximated above (for γ_{fd}, see Connelly et al., 1997). This procedure corresponds to probing one acceptor per LHC-II monomer, i.e., $N_A = 1$ in Eq. 3. The contribution of $\sigma^{em}(\omega_p)$ can be obtained as the difference of both spectra (see Fig. 6), resulting in a maximum value of $1.0(\pm0.2) \times 10^{-15}$ cm^2 at 683 nm. However, applying the same procedure assuming $N_A = 2$ yields the unreasonably high value of 3.6×10^{-15} cm^2 for $\sigma^{em}(\omega_p)$ at maximum. Therefore, we conclude that only the case $N_A = 1$ is in agreement with the experimental data. The emission spectrum $\sigma^{em}(\omega_p)$ obtained from ξ-spectrum analysis is centered at 683 ($\pm$1) nm and can be approximated by a Gaussian with 260 ($\pm$30) cm^{-1} FWHM (see Fig. 6). Notably, the fluorescence spectrum of LHC-II has a broader width and a non-Gaussian shape. Deconvolution of the fluorescence spectrum, considering one Gaussian as obtained from the ξ-spectrum, suggests the existence of an additional fluorescence band centered at ~672 nm. This band contributes less than 40% to the total fluorescence yield (see Fig. 7). The additional fluorescent species is completely lacking in the ξ-spectrum, because it originates from acceptor(s) with vanishing contributions at probe wavelength of 685 nm.

DISCUSSION

According to the used model, the result $N_A = 1$ implies that, within a LHC-II monomeric subunit, only one state emits at a given time in the main fluorescence region above 680 nm. Hence, while one branch in the EET chain is obviously directed to an emitter at ~672 nm, no further permanent branches appear to exist. A temporarily fluctuating acceptor (for example, due to spectral shifts) cannot be excluded explicitly, if only one branch is active at the same time. In this case, however, the cross section as obtained by NLPF still corresponds to only one transition—the one with the lowest saturation threshold. The measured value of the maximum emission cross section at 683 nm of LHC-II is 3.2 times that of monomeric Chl *a*. Moreover, a 4.2-fold increased absorption cross section for a subband at the red edge of the Q_y-region was found in the NLA experiment. As illustrated in Fig. 6, both increased cross sections most probably belong to the same electronic transition, in particular, if a Stokes-shift similar to that observed for Chl *a* in solution is assumed. The remaining deviation in the cross sections as obtained by the two approaches is due to the experimental error, and the mean value suggests a 3.7($\pm$1)-fold increased cross section as compared to Chl *a* in solution.

Reasonable explanations for the increased maximum cross section can be either line narrowing in the protein environment or size enhancement of the corresponding transition-dipole moment. The effect of line narrowing can be estimated by comparing the line width of the emitting subband of LHC-II with that of the Q_y-(0−0) vibrational band of Chl *a* in solution (390 cm^{-1} FWHM; Shipman, 1977). As illustrated in Fig. 7, the width of the emission band obtained by NLPF is 260(±30) cm^{-1} (FWHM). This is slightly higher than the previously reported value of 220 cm^{-1} for the FWHM of subbands in the red absorption region of LHC-II (Zuchelli et al., 1996). However, the FWHM as obtained by Zuchelli et al. (1996) was estimated indirectly by deconvolution of the absorption spectrum into Gaussian subbands, the outcome of which depends strongly on the assumed substructure model. To account for the uncertainty of the linewidth, in the following calculations, we use an average value of 240 cm^{-1} with an error range of ±40 cm^{-1}. Under this assumption, a 2.3(±0.8)-fold size enhancement of the transition-dipole strength can be derived. The most obvious reason for such an enhancement is redistribution of oscillator strength by excitonic interaction between Chl molecules, thus forming the terminal emitter in LHC-II. The magnitude of redistribution depends, thereby, on the interacting Chl species, the distance between them and the geometrical arrangement of their transition dipoles (van Amerongen et al., 2000). Hence, this coupling involves at least two Chls, assuming that all Q_y-oscillator strength of both molecules is redistributed to the lower exciton state.

In a recent study, Rogl and Kühlbrandt (1999) reported the assignment of the lowest Chl *a* transition at ~680 nm to the Chl-binding site **a2**. (Please note that the designation of Chl-binding sites in this paper refers to the original nomenclature of Kühlbrandt et al. (1994). These must not necessarily correspond to Chls *a* and *b*, because a few reassignments (see, e.g., Rogl and Kühlbrandt, 1999) had to be introduced recently.) In contrast, theoretical calculations of the Q_y-transition energies for Chls in LHC-II, considering their unique (binding-site dependent) environment, resulted in a value of only 670 nm for Chl **a2** (14,918 cm^{-1} for attachment to the Asparagin residue, see Nishigaki et al., 2001). For that reason, an additional mechanism, like excitonic coupling, must be responsible for the experimentally observed shift of Chl **a2** to ~680 nm. Furthermore, the existing structural model shows that the shortest center-to-center distance between two Chls in LHC-II is that of Chl **a2** and **b2** with 8.3 Å (Kühlbrandt et al., 1994). Therefore, the size enhancement of the transition-dipole strength of the terminal emitter is discussed in the following section with respect to possible excitonic coupling of Chl **a2** to its nearest neighbors.

The three-dimensional structure allows the estimation of the mutual orientations of the corresponding Chl molecular planes, although the orientations of the transition dipoles within these planes are not determined, yet. Assuming that the dipole moments are oriented along the diagonals of their tetrapyrrole rings, a binary model for the orientations was developed by Gradinaru et al. (1998). Based on this, van Amerongen and van Grondelle (2001) presented calculations of excitonic coupling strengths for all Chl sites, yielding the highest value of $V_{a2/b2}$ = 121 cm^{-1} for the Chl **a2**/**b2** pair. This value, however, is insufficient for the formation of delocalized excitonic states. Kimura et al. (2000) have outlined the approximate condition for exciton delocalization as $4V > 3\Gamma$, where V is the coupling strength and Γ is the homogeneous linewidth caused by dynamic disorder. For Γ = 185 cm^{-1} (Zuchelli et al., 1996) and $V_{a2/b2}$ = 121 cm^{-1}, this condition is obviously not fulfilled. Hence, for the diagonal orientation of the transition dipoles within the tetrapyrrole ring, a size enhancement by excitonic coupling cannot be explained.

Several attempts have been made to determine the exact orientation of the Q_y- and Q_x-transition dipole moments of Chls within their molecular frames. Vrieze and Hoff (1995) have described the orientation of the Q_y transition in Chl *a* as being rotated by ~20° out of the diagonal in the tetrapyrrole ring. A similar value was recently used by Simonetto et al. (1999) for determination of the Chl orientations in the minor antenna complex CP29. Although the question remains whether this angle is conserved for Chls bound to a protein matrix, it provides four new reasonable configurations of the mutual dipole arrangement of the Chls **a2** and **b2**, which are worthy of investigation. As it turns out, one of these orientations increases the calculated dipole–dipole interaction energy considerably. In this configuration, the Q_y-transition dipoles of Chl **a2** and **b2** are oriented nearly in one plane with the center-to-center distance vector and enclose an angle of only 23°. Following the calculation procedure used by van Amerongen and van Grondelle (2001), this configuration results in a larger geometrical factor κ = 1.38, and thus yields $V_{a2/b2}$ = 181 cm^{-1}.

The center wavelength of the Q_y-(0−0) transition band of Chl *a* in a protein environment was experimentally determined at 668 nm (Kleima et al., 2000), which corresponds sufficiently to the calculation for Chl **a2** by Nishigaki et al. (2001). Assuming the same spectral shift, a value of ~648 nm can be obtained for Chl *b* within the protein. Basing on the coupling and geometry as obtained above, these values yield, in the calculation according to van Amerongen et al. (2000), the following two excitonic subbands: one centered at 671 nm with 1.6-times the dipole strength of monomeric Chl *a* and another one at 645 nm with less than 0.4-times the dipole strength of Chl *b*. This model of an excitonically coupled Chl *a*/*b* heterodimer fits the lower limit (1.5-fold) of the obtained size enhancement of the acceptor species. Nevertheless, the calculated shift by only 3 nm is not consistent with the experimental results—i.e., under the assumption of the uncoupled Chl *a* transitions being centered at 668 nm.

At this point, it is interesting to note that the assignment of Chl *a* or Chl *b* to the distinct binding sites in the structural model has been made only tentatively, i.e., relying on the

necessity of Chl *a* triplet state quenching by carotenoids (Kühlbrandt et al., 1994). For several of the binding sites, the occupation with either Chl *a* or Chl *b* has been confirmed by analysis of reconstituted complexes from apoproteins in which individual Chl-binding amino acid residues had been removed by site-directed mutagenesis (Rogl and Kühlbrandt, 1999). In contrast, occupation of site **b3** by Chl *a* was also verified therein. Remarkably, Chl **b2** is one of three chromophores in LHC-II for which no Mg-coordinating amino-acid residue can be defined in the protein sequence. The presumed occupation by Chl *b* can thus not be checked by site-directed mutagenesis. Hence, in principle, an alternative assignment of this chromophore to Chl *a* is conceivable. Excitonic calculations of a tentative Chl *a* homodimer located at sites **a2** and **b2** with the favorable geometry as described above yields a coupling strength of 216 cm^{-1}. This would result in one transition at 678 nm with dipole strength of 1.9 times that of monomeric Chl *a* and another one at 659 nm with less than 8% of the dipole strength of Chl *a*.

For both models, the homo- and the heterodimer, the dipole–dipole interaction, fulfills the condition for exciton delocalization $4V > 3\Gamma$ using $\Gamma = 185$ cm^{-1} according to Zuchelli et al. (1996). Interestingly, this relation still holds for $\Gamma = 240$ cm^{-1}, a value that is higher than the maximum Γ consistent with the total FWHM of the subband (see above). In contrast, the calculated coupling strength to further neighbors of Chl **a2** in the frame of the present structural model did not suffice to meet the delocalization criterion. For example, the Chl **a2**/**a1** interaction amounts to only 26 cm^{-1}. Although, at a first glance, calculations assuming a homodimer fit the experimentally obtained values better than a heterodimer, we have to consider a possible hyperchromic effect redistributing oscillator strength from the Soret band into the Q_y band. Such an effect has been observed to accompany strong excitonic interaction between Chls *a* in aggregates as formed in 50% aqueous DMSO (Schubert et al., 1998). For this system, assumed to consist of dimeric subunits, redistribution of oscillator strength from the Soret to the Q_y band on the order of 30% has been observed. Such hyperchromism has also been discussed for the highly related bacteriochlorophylls, e.g., by Scherz and Parson (1984). A hyperchromic effect of comparable magnitude would further increase the calculated transition dipole of the lower excitonic state in the case of the heterodimer to a factor of ~2. Unfortunately, a quantitative calculation of hyperchromic oscillator-strength redistribution is impossible without detailed knowledge about the energy levels in the Soret region. Hence, we cannot reliably determine the type of the dimer in this study. Recent results obtained by evaluation of stepwise two-photon excited fluorescence from the B_x state (Soret band), however, gave strong hints for the existence of a Chl *a*/*b* heterodimer in LHC-II, probably located at the sites **a2**/**b2** (D. Leupold, K. Teuchner, J. Ehlert, K.-D. Irrgang, G. Renger, and H. Lokstein, submitted for publication). Under this assumption, the deviation in the exciton band position for the Chl *a*/*b* heterodimer as calculated above (671 nm) necessitates a larger spread of the original (molecular) transition energies due to pigment–protein interactions (compare Nishigaki et al., 2001).

The findings of a strong absorber/emitter at the red edge of the Q_y-absorption band are further consistent with the first results from single molecule spectroscopy of LHC-II (Tietz et al., 2001) and linear dichroism measurements (Nussberger et al., 1994). In temperature-dependent circular dichroism spectra of LHC-II (Hemelrijk et al., 1992) the strongest feature appears between 676 and 685 nm. This may well indicate the existence of an excitonic band in this region. Any corresponding higher energetic excitonic transition, however, was not identified due to the nonconservative structure of the circular dichroism spectrum and the probable superposition of several bands.

CONCLUSIONS

In the current study, evidence is provided for excitonic coupling of Chls in LHC-II absorbing in the red edge of the Q_y-absorption region. Moreover, the proposed Chl dimer can be related to the Chl-binding sites **a2** and **b2** in the LHC-II structure (Kühlbrandt et al., 1994) using the recent assignment of Rogl and Kühlbrandt (1999) and the calculations of coupling strengths. In this framework, two possibilities, an excitonically coupled Chl *a* homodimer or the Chl *a*/*b* heterodimer, are consistent with the experimental results. Apparently, the Chl **a2**/**b2** pair is located on the outer surface of the LHC-II complex even in its trimeric form. The absorption of the pair is shifted to the red edge of the Q_y band by excitonic interaction. Hence, this pair appears to function as a "trapping state" of the complex, and the EET to neighboring LHC-II trimers occurs mainly here. The size enhancement of the transition dipole can potentially increase the connectivity of neighboring trimers, thus contributing to the formation of an extended PS II-antenna network. Additionally, the enhanced dipole moment may also attract electronic excitations from inside the antenna to the surface. The fluorescent dimer at the end of the LHC-II EET chain is therefore expected to play a crucial role for the overall efficiency of higher plant photosynthetic energy conversion.

APPENDIX

The NLPF-signal dependence on probe frequency (ω_t), pump frequency (ω_p), and pump-field intensity (I_p) can be expressed in general as

$$S(\omega_t, \omega_p, I_p) \propto \left| \int_0^{\pi} d\theta \sin^5\theta \int_0^{2\pi} d\phi \cos^2\phi \cos 2\phi \times \sum_{ij} \zeta_{ij}(\omega_t)(n_i - n_j) \right|^2, \quad \text{(A1)}$$

with Re $\zeta_{ij}(\omega) = \sigma_{ij}(\omega)/2$, Im $\zeta_{ij}(\omega) = \sigma_{ij}(\omega)(\omega - \omega_{ij})/2\Gamma_{ij}$ (Beenken and May, 1997). The integrals average over randomly oriented dipoles (sample

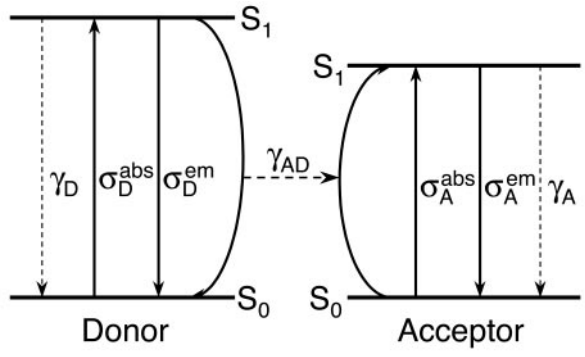

FIGURE A1 Term scheme used for description of intensity-dependent NLPF. γ_{AD} is the EET rate between Donor (D) and Acceptor (A). γ_D and γ_A are the energy relaxation rates. Parameters σ^{abs} and σ^{em} indicate the corresponding absorption and emission cross sections.

representation) characterized by the angles ϕ and θ. The population probabilities n_j are determined by the following system of equations:

$$\sum_j (\gamma_{ij} + \sigma_{ij}(\omega_p) I_p \sin^2\theta \cos^2\phi) n_j = 0. \qquad \text{(A2)}$$

The energy relaxation rate and cross section of the transition from state j to i are termed γ_{ij} and $\sigma_{ij}(\omega_p)$, respectively. The diagonal elements γ_{ii} and $\sigma_{ii}(\omega)$ are given by

$$\gamma_{ii} = -\sum_j \gamma_{ji}$$

and

$$\sigma_{ii}(\omega_p) = -\sum_j \sigma_{ji}(\omega_p). \qquad \text{(A3)}$$

Thus, Eq. A2 would be singular without the constriction $\Sigma_j n_j = 1$. The development of a model adequate to the investigated species LHC-II is based on description of the EET process for a donor–acceptor (D–A) pair, which is further generalized to a multiple D–A scheme with branched energy transfer. Both D and A can be represented by two-level systems (see Fig. A1), if higher excited-states are not saturated (because of a lifetime much shorter than the ground-state recovery time, Beenken and Ehlert, 1998). This assumption is fulfilled for Chls (also in LHC-II) due to the ultrashort lifetimes of typical porphyrins higher excited singlet states (cf. Cho et al., 1999).

For the system in Fig. A1, the matrices from Eqs. A1 and A2 can be expressed as

$$\hat{\gamma} = \begin{pmatrix} 0 & \gamma_A & \gamma_D & 0 \\ 0 & -\gamma_A & \gamma_{AD} & \gamma_D + \gamma_{ann} \\ 0 & 0 & -\gamma_D - \gamma_{AD} & \gamma_A + \gamma_{ann} \\ 0 & 0 & 0 & -\gamma_A - \gamma_D - 2\gamma_{ann} \end{pmatrix}$$

$$\hat{\sigma}(\omega) = \begin{pmatrix} -\sigma_A^{abs}(\omega) - \sigma_D^{abs}(\omega) & \sigma_A^{em}(\omega) & \sigma_D^{em}(\omega) & 0 \\ \sigma_A^{abs}(\omega) & -\sigma_A^{em}(\omega) - \sigma_D^{abs}(\omega) & 0 & \sigma_D^{em}(\omega) \\ \sigma_D^{abs}(\omega) & 0 & -\sigma_A^{abs}(\omega) - \sigma_D^{em}(\omega) & \sigma_A^{em}(\omega) \\ 0 & \sigma_D^{abs}(\omega) & \sigma_A^{abs}(\omega) & -\sigma_A^{em}(\omega) - \sigma_D^{em}(\omega) \end{pmatrix}. \qquad \text{(A4)}$$

The first, second, and third row represent processes that populate (+) or depopulate (−) the ground states and the excited states of the acceptor (A) and the donor (D), respectively. The fourth row indicates excitation of both, D and A. The processes correspond to absorption of the acceptor ($\sigma_A^{abs}(\omega)$) and the donor ($\sigma_D^{abs}(\omega)$), stimulated emissions to the ground states ($\sigma_A^{em}(\omega)$, $\sigma_D^{em}(\omega)$), and the energy-relaxation rates (γ_A, γ_D). EET from D to A is represented by the rate γ_{AD}. EET rates measured in LHC-II are significantly higher than the fluorescence decay rate, which corresponds, in our model, to the energy relaxation rate of an acceptor. Hence, the approximation $\gamma_{AD} \gg \gamma_A \approx \gamma_D$ can be introduced in the further calculation. The third column of matrix $\hat{\gamma}$ contains the excitation-annihilation rate γ_{ann}. It describes the rate for generation of one doubly excited state for simultaneously excited D and A and the subsequent relaxation of this doubly excited state into a single-excited one. Resulting from fast EET and short lifetimes of higher excited states of Chls in LHC-II, this annihilation rate of a D–A pair is considerably higher than the relaxation rate of the first excited state. Hence, the approximation $\gamma_{ann} \gg \gamma_A \approx \gamma_D$ can be introduced in what follows. Finally, we restrict the model to intensities lower than the saturation threshold of the donor, which is much higher than that of the acceptor due to annihilation and fast EET: $\gamma_{ann}, \gamma_{AD} \gg \sigma_D^{abs} I \approx \sigma_D^{em} I$. With these approximations, Eqs. A1–A4 yield the intensity-dependent NLPF signal,

$$\begin{aligned} S(\omega_t, \omega_p, I_p) &\propto \left| \int_0^{\pi} d\theta \sin^3\theta \int_0^{2\pi} d\phi \cos 2\phi \, \zeta_A(\omega_t) \right. \\ &\times \frac{\sigma_A^{abs}(\omega_p) + \sigma_D^{abs}(\omega_p)}{\gamma_A} \\ &\times \left(\frac{15}{13} \eta(\omega_t, \omega_p) + \frac{1}{1 + \xi(\omega_p) I_p \sin^2\theta \cos^2\phi} \right) \\ &\left. \times I_p \sin^2\theta \cos^2\phi^2, \right. \end{aligned} \qquad \text{(A5)}$$

containing the saturation parameter

$$\xi(\omega_p) = \frac{\sigma_D^{abs}(\omega_p) + \sigma_A^{abs}(\omega_p) + \sigma_A^{em}(\omega_p)}{\gamma_A}. \qquad \text{(A6)}$$

The saturation parameter is the quantity of interest in this study, because it allows determination of absolute cross sections, if γ_A is known. The second parameter,

$$\eta(\omega_p) = \frac{13}{15}\frac{\sigma_D^{abs}(\omega_p)}{\sigma_A^{abs}(\omega_p) + \sigma_D^{abs}(\omega_p)} \times \frac{\gamma_A}{\gamma_{AD}}, \qquad (A7)$$

contains the ratio γ_A/γ_{AD} and thus allows verification of the basic approximation used, $\gamma_{AD} \gg \gamma_A$. Evaluating the integrals for orientation averaging, the intensity dependence of the NLPF signal is given by

$$S(\omega_t, \omega_p, I_p) \propto \left| \eta(\omega_t, \omega_p)\xi(\omega_p)I_p + \frac{3}{\xi(\omega_p)I_p} - \left(1 + \frac{3}{\xi(\omega_p)I_p}\right)\frac{\arctan\sqrt{\xi(\omega_p)I_p}}{\sqrt{\xi(\omega_p)I_p}} \right|^2. \qquad (A8)$$

This result can be easily extended to systems with more than one donor substituting σ_D^{abs} by a sum of cross-sections $\Sigma_D\, \sigma_D^{abs}$ in Eq. A6. Considering more than one acceptor species (not unlikely for antenna complexes), summation over several σ_A^{abs} and σ_A^{em} can also be introduced. However, in this case, the overall fluorescence decay rate has to be multiplied with the number of the probed terminal acceptors (N_A), which corresponds to the effective number of branches in the EET path. Using the reasonable approximation of similar fluorescence decay rates for every acceptor, the saturation parameter yields

$$\xi(\omega_p) = \frac{\sum_D \sigma_D^{abs}(\omega_p) + \sum_A \sigma_A^{abs}(\omega_p) + \sum_A \sigma_A^{em}(\omega_p)}{N_A \cdot \gamma_{fd}}. \qquad (A9)$$

In other words, the quantity $\xi(\omega_p)$ correlates with the combined absorption and emission cross sections "per terminal state of the EET chain."

We gratefully acknowledge collaboration with the Max-Born-Institut Femtosecond-Laser Application Laboratory (Dr. F. Noack) and helpful discussions about LHC-II structure with Dr. H. Rogl (MPI für Biophysik, Frankfurt, Germany).

Financial support by the Deutsche Forschungsgemeinschaft (Le 729/2-3 and Ho 1757/2-2, and SFB 429, TP A2) is also acknowledged.

REFERENCES

Agarwal, R., B. P. Krueger, G. D. Scholes, M. Yang, J. Yom, L. Mets, and G. R. Fleming. 2000. Ultrafast energy transfer in LHC-II revealed by three-pulse photon echo peak shift measurements. *J. Phys. Chem. B.* 104:2908–2918.

Beenken, W., and J. Ehlert. 1998. Subband analysis of molecular electronic transitions by nonlinear polarization spectroscopy in the frequency domain. *J. Chem. Phys.* 109:10126–10137.

Beenken, W., and V. May. 1997. Strong field theory of nonlinear polarization spectroscopy. Fundamentals and the two-level system. *J. Opt. Soc. Am. B.* 14:2804–2810.

Cho, H. S., N. W. Song, Y. H. Kim, S. C. Jeoung, S. Hahn, D. Kim, S. K. Kim, N. Yoshida, and A. Osuka. 2000. Ultrafast energy relaxation dynamics of directly linked porphyrin arrays. *J. Phys. Chem. A.* 104: 3287–3298.

Connelly, J. P., M. G. Müller, M. Hucke, G. Gatzen, C. W. Mullineaux, A. V. Ruban, P. Horton, and A. R. Holzwarth. 1997. Ultrafast spectroscopy of trimeric light-harvesting complex II from higher plants. *J. Phys. Chem. B.* 101:1902–1909.

Gradinaru, C. C., S. Özdemir, D. Gülen, I. H. M. van Stokkum, R. van Grondelle, and H. van Amerongen. 1998. The flow of excitation energy in LHCII monomers: implications for the structural model of the major plant antenna. *Biophys. J.* 75:3064–3077.

Hemelrijk, P. W., S. L. S. Kwa, R. van Grondelle, and J. P. Dekker. 1992. Spectroscopic properties of LHC-II, the main light-harvesting chlorophyll *a*/*b* protein complex from chloroplast membranes. *Biochim. Biophys. Acta.* 1098:159–166.

Kimura, A., T. Kakitani, and T. Yamato. 2000. Theory of excitation energy transfer in the intermediate coupling case. II. Criterion for intermediate coupling excitation energy transfer mechanism and application to the photosynthetic antenna system. *J. Phys. Chem. B.* 104:9276–9287.

Kleima, F. J., M. Wendling, E. Hofmann, E. J. G. Peterman, R. van Grondelle, and H. van Amerongen. 2000. Peridinin chlorophyll *a* protein: Relating structure and steady-state spectroscopy. *Biochemistry.* 39:5184–5195.

Krupa, Z., N. P. A. Huner, J. P. Williams, E. Maissan, and D. R. James. 1987. Development at cold-hardening temperatures. *Plant Physiol.* 84: 19–24.

Kühlbrandt, W., D. N. Wang, and Y. Fujiyoshi. 1994. Atomic model of plant light-harvesting complex by electron crystallography. *Nature.* 367: 614–621.

Leupold, D., H. Stiel, K. Teuchner, F. Nowak, W. Sandner, B. Ücker, and H. Scheer. 1996. Size enhancement of transition dipoles to one- and two-exciton bands in a photosynthetic antenna. *Phys. Rev. Lett.* 77: 4675–4677.

Leupold, D., H. Stiel, J. Ehlert, F. Nowak, K. Teuchner, B. Voigt, M. Bandilla, B. Uecker, and H. Scheer. 1999. Photophysical characterization of the B800-depleted light harvesting complex B850 of *Rhodobacter sphaeroides*. Implications to the ultrafast energy transfer 800→850 nm. *Chem. Phys. Lett.* 301:537–545.

Lokstein, H., D. Leupold, B. Voigt, F. Nowak, J. Ehlert, P. Hoffmann, and G. Garab. 1995. Nonlinear polarization spectroscopy in the frequency domain of light-harvesting complex II: absorption band substructure and exciton dynamics. *Biophys. J.* 69:1536–1543.

Lokstein, H., A. Schubert, B. Voigt, and D. Leupold. 1998. Direct resolution of spectral fine-structure and ultrafast exciton dynamics in light-harvesting complex II by nonlinear polarization spectroscopy in the frequency domain. *In* Photosynthesis: Mechanisms and Effects. Vol. I., G. Garab, editor. Kluwer, Dordrecht, The Netherlands. 293–296.

Nishigaki, A., S. Ohshima, K. Nakayama, M. Okada, and U. Nagashima. 2001. Application of molecular orbital calculations to interpret the chlorophyll spectral forms in pea photosystem II. *Photochem. Photobiol.* 73:245–248.

Nussberger, S., J. P. Dekker, W. Kühlbrandt, B. M. van Bolhuis, R. van Grondelle, and H. van Amerongen. 1994. Spectroscopic characterization of three different monomeric forms of the main chlorophyll *a*/*b* binding protein from chloroplast membranes. *Biochemistry.* 33:14775–14783.

Reddy, N. R. S., H. van Amerongen, S. L. S. Kwa, R. van Grondelle, and G. J. Small. 1994. Low-energy exciton level structure and dynamics in light harvesting complex II trimers from the Chl *a*/*b* antenna complex of photosystem II. *J. Phys. Chem.* 98:4729–4735.

Remelli, R., C. Varotto, D. Sandonà, R. Croce, and R. Bassi. 1999. Chlorophyll binding to monomeric light-harvesting complex. *J. Biol. Chem.* 274:33510–33521.

Rogl, H., and W. Kühlbrandt. 1999. Mutant trimers of light-harvesting complex II exhibit altered pigment content and spectroscopic features. *Biochemistry.* 38:16214–16222.

Sauer, K., J. R. L. Smith, and A. J. Schultz. 1966. The dimerization of chlorophyll *a*, chlorophyll *b*, and bacteriochlorophyll in solution. *J. Am. Chem. Soc.* 88:2681–2688.

Scherz, A., and W. W. Parson. 1984. Exciton interactions in dimers of bacteriochlorophyll and related molecules. *Biochim. Biophys. Acta.* 766: 666–678.

Schubert, A., B. Voigt, D. Leupold, W. Beenken, J. Ehlert, P. Hoffmann, and H. Lokstein. 1997. Direct observation of spectral substructure in the Q_y-absorption band of light harvesting complex II by nonlinear polari-

sation spectroscopy in the frequency domain at low temperature. *Biochim. Biophys. Acta.* 1321:195–199.

Schubert, A., M. A. Krikunova, H. Stiel, J. Ehlert, D. Leupold, and H. Lokstein. 1998. Determination of the aggregate size in chlorophyll *a* oligomers by nonlinear absorption spectroscopy on the ps and fs timescale. *In* Photosynthesis: Mechanisms and Effects. Vol. I., G. Garab, editor. Kluwer, Dordrecht, The Netherlands. 469–472.

Shipman, L. 1977. Oscillator and dipole strengths for chlorophyll and related molecules. *Photochem. Photobiol.* 26:287–292.

Simonetto, R., M. Crimi, D. Sandona, R. Croce, G. Cinque, J. Breton, and R. Bassi. 1999. Orientation of chlorophyll transition moments in the higher-plant light-harvesting complex CP29. *Biochemistry*. 38: 12974–12983.

Song, J. J., J. H. Lee, and M. D. Levenson. 1978. Picosecond relaxation measurements by polarization spectroscopy in condensed phases. *Phys. Rev. A.* 17:1439–1447.

Stiel, H., W. Becker, and K. Teuchner. 1991a. Spectrometer for nonlinear absorption measurements using a software-controlled signal analyzer. *Exp. Techn. Physik.* 39:15–24.

Stiel, H., K. Teuchner, D. Leupold, S. Oberländer, J. Ehlert, and R. Jahnke. 1991b. Computer aided laser-spectroscopic characterization and handling of molecular excited states. *Intell. Instrum. Comp.* 9:79–87.

Tietz, C., F. Jelezko, U. Gerken, S. Schuler, A. Schubert, H. Rogl, and J. Wrachtrup. 2001. Single molecule spectroscopy on the light-harvesting complex II of higher plants. *Biophys. J.* 81:556–562.

Trinkunas, G., J. P. Connelly, M. G. Müller, L. Valkunas, and A. Holzwarth. 1997. Model for the excitation dynamics in the light-harvesting complex II from higher plants. *J. Phys. Chem. B.* 101:7313–7320.

Van Amerongen, H., L. Valkunas, and R. van Grondelle. 2000. Photosynthetic Excitons. World Scientific Publishing, Singapore.

Van Amerongen, H., and R. van Grondelle. 2001. Understanding the energy transfer function of LHC-II, the major light-harvesting complex of green plants. *J. Phys. Chem. B.* 105:604–617.

Van Grondelle, R. 1985. Excitation energy transfer, trapping and annihilation in photosynthetic systems. *Biochim. Biophys. Acta.* 811:147–195.

Vrieze, J., and A. J. Hoff. 1995. The orientation of the triplet axes with respect to the optical-transition moments in (bacterio)chlorophylls. *Chem. Phys. Lett.* 237:493–501.

Voigt, B., F. R. Nowak, and W. Beenken. 1999. A new set-up for nonlinear polarization spectroscopy in the frequency domain: experimental examples and theoretical background. *Meas. Sci. Technol.* 10:N7–N11.

Zucchelli, G., F. M. Garlaschi, and R. C. Jennings. 1996. Thermal broadening analysis of the light harvesting complex II absorption spectrum. *Biochemistry*. 35:16247–16254.